ICAS-84-1.8.3

AERODYNAMIC INVESTIGATIONS ON AN ADAPTIVE AIRFOIL FOR A TRANSONIC TRANSPORT AIRCRAFT

G. Redeker G. Wichmann
Deutsche Forschungs- und Versuchsanstalt
für Luft- und Raumfahrt e.V. (DFVLR)
Institut für Entwurfsaerodynamik

H.-Chr. Oelker
Technische Universität Braunschweig
Institut für Strömungsmechanik

Abstract

Drag reduction and the extension of the flight region with high aerodynamic efficiency for transonic airfoils has been investigated by applying the idea of an adaptive airfoil. With the aid of the elliptic continuation method a basic airfoil has been optimized with regard to shockfree pressure distributions for three different sets of Mach number and lift coefficient. The resulting three airfoils, representing an adaptive airfoil, have been investigated numerically and in windtunnel tests. The results indicate that high aerodynamic efficiencies are connected with pressure distributions having already weak shockwaves. Furthermore the anticipated extension of the flight region with high aerodynamic efficiency by applying an adaptive airfoil could not be verified for all flight conditions.

Notation

x,y	coordinate system
c	airfoil chord
a	speed of sound
a^*	speed of sound at critical state
V_∞	velocity of freestream flow
$\vec{V}$	local velocity vector
$q = \lvert\vec{V}\rvert$	Value of local velocity vector
Re	Reynolds number based on airfoil chord
$M=V_\infty/a$	freestream Mach number
α	angle of attack
c_l	lift coefficient
c_{lD}	lift coefficient at design condition
c_d	drag coefficient
c_{dW}	wave drag coefficient
$M \cdot c_l/c_d$	aerodynamic efficiency
c_p	static pressure coefficient
c_p^*	static pressure coefficient at critical state
p_0	total pressure of freestream
p_{01}	total pressure in the airfoil wake
$\varkappa$	isentropic exponent
ρ	density of air
ρ^*	density of air at critical state
δ^*	boundary layer displacement thickness
P	exponent in equ. (2)

1. Introduction

Due to drastic rise in fuel prices the direct operating costs (DOC) of commercial transport aircraft have increased considerably [1]. Therefore new concepts for reducing DOC and fuel saving research programs have been established worldwide [2, 3,4] by applying new technologies in aerodynamics, structures and materials, propulsion technique and flight guidance and control for aircraft. The predicted fuel savings range from 4% to 10% at short sight and 20% to 40% in the future.

For the new generation of transport aircraft, which has gone into service now (e.g. Airbus A310 and Boeing 757/767) the transonic wing technology has been applied as aerodynamic means to increase the aircraft performance and to save fuel. The basic ideas and the benefits of transonic wing technology have been discussed extensively [5,6] and should not be repeated here.

This paper deals with the possibility of a further improvement of the transonic wing by considering so-called adaptive airfoils to extend the economic flight regime by adjusting the airfoil contour for optimum wing performances at different flight conditions. In the following a short description of the basic ideas of adaptive airfoils will be discussed, the methods used for the airfoil design will be outlined and finally experimental results of such an airfoil will be presented.

2. Principles of an adaptive airfoil

As the aerodynamic behaviour of high aspect ratio wings of transport aircraft is mainly influenced by the wing section generating the wing contour this basic wing section plays an important role in the wing design process. Therefore concentration of research work on improvements in airfoil performance is reasonable for transport aircraft and is highly influencing the success of a wing design [7]. The new generation airfoils for transport aircraft, transonic airfoils, mostly are optimized for one design point of the wing, namely the cruise condition. In order to minimize the drag of the airfoil at the design point a pressure distribution with no shockwaves terminating the supersonic region or pressure distributions with only weak shockwaves were chosen thus reducing or suppressing the wave drag [8].

The experiences with transonic airfoils show that real shockfree pressure distribu-

tions can only be achieved in one singular point concerning Mach number and lift coefficient, e.g. the design point. At off-design conditions above or below this point shockwaves of different strength may occur leading to increased drag. Whereas in analysis calculations shockfree pressure distributions could be verified, experimental

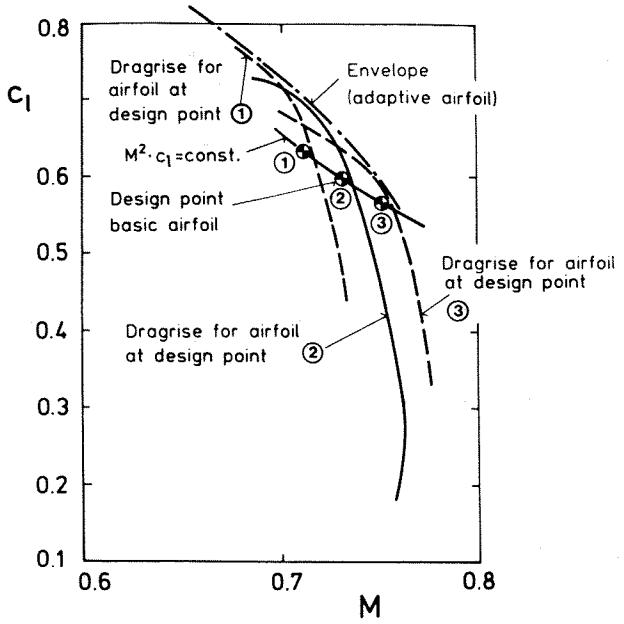

Fig. 1 Expected dragrise curve for an adaptive airfoil

results always show near the design conditions weak shockwaves. This demonstrates that the shockfree design pressure distribution is a singular point which could not be achieved in experiments. On the other hand it can be stated that measured pressure distributions with weak shockwaves near the design condition do not suffer from additional drag penalties [6]. But in off-design conditions the shock strength can grow rapidly causing undesirable drag increments.

This situation is not without problems for the operational conditions of a transport aircraft as the flight conditions at cruise cannot be matched always with the design conditions because the aircraft often is forced to fly at other conditions than those with optimum performances. This can be due to changes in flight level and flight speed coming from operational contraints of flight safety.

This demonstrates the necessity to apply an airfoil with optimum performance in a certain region of Mach number and lift coefficient. To achieve this goal the following possibilities may be considered:

- development of an airfoil with a certain region of good performance but with a reduction in performance compared to an optimized airfoil for one flight condition or
- making use of a so-called adaptive airfoil as proposed by Sobieczky, Fung, Seebass [9].

An adaptive airfoil is equipped with a flexible upper surface contour which can be adjusted for different flow conditions in that way that always shockfree pressure distributions can be achieved thus resulting always with an optimum airfoil performance. This will lead to an extended flight regime as it is demonstrated schematically in a Mach number lift coefficient diagram for the dragrise curve in Fig. 1. It is expected that the dragrise curve for the adaptive airfoil is generated by the envelope of the dragrise curves of several optimized airfoils with the same basic shape with various design points. The case presented in Fig. 1 shows three airfoil variations with different Mach numbers and constant lift force, e.g. $M^2 \cdot c_l$ = const..

As up to now only theoretical considerations have been made on this subject [9] a combined theoretical and experimental investigation has been carried out at the Institute for Design Aerodynamics of DFVLR, Braunschweig. This investigation is not aimed for providing hardware solutions for a flexible upper surface airfoil contour, but will concentrate on the aerodynamic behaviour of such an airfoil. Therefore the adaptive airfoil is split up into three separate airfoils having the same shape with the exception of a certain portion of the upper surface contour, which still has to be designed. These airfoils represent three flow conditions of an adaptive air-

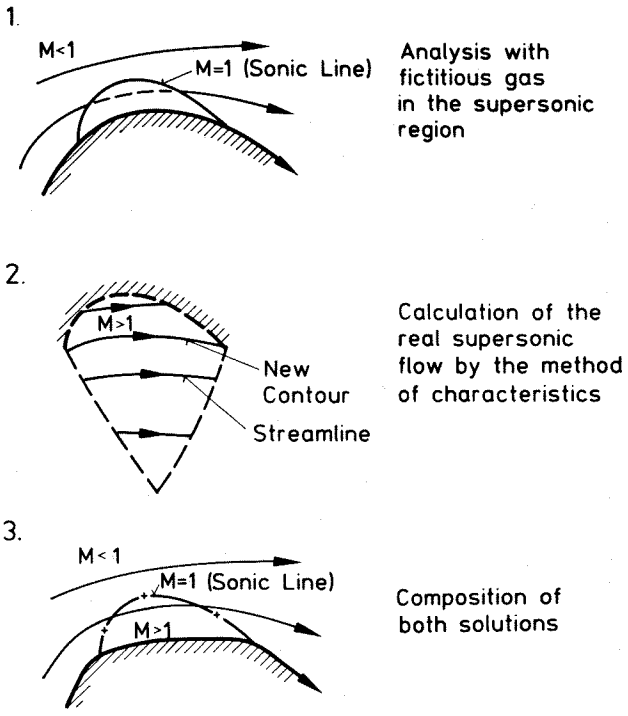

Fig. 2 Principle of the method of elliptic continuation for transonic airfoils

foil with shockfree pressure distributions at the design lift coefficients for a Mach number range of $0.71 \leq M \leq 0.75$. The design lift coefficients corresponding to the Mach numbers M = 0.71, 0.73 and 0.75 are aimed for to vary with $M^2 \cdot c_l = \text{const.}$ giving a constant lift force.

Having specified the problem now the difficulty remains to provide an airfoil with upper surface contours which under prescribed conditions show shockfree pressure distributions. This problem is solved by the "elliptic continuation method" which will be discussed next.

3. Method of Elliptic Continuation

The principle of the method of elliptic continuation was first introduced by Sobieczky [10] and Eberle [11]. The basic ideas are demonstrated in Fig. 2. At transonic flow conditions the flowfield around an airfoil with an embedded supersonic region can be solved by the full potential equation, which is outside the supersonic region of elliptical type and inside of hyperbolic type. This mixed type of flowfield is one of the major difficulties for solving the full potential equation. Furthermore the supersonic region is normally terminated by a shockwave. The occurrence of this shockwave can be suppressed if the type of potential equation is artificially changed to elliptical behaviour in the supersonic region, too. This can be accomplished by introducing into the analysis code for solving the full potential equation a fictitious gas law [12]. The correct density relationship of isentropic flow

$$\left[\frac{\rho}{\rho^*}\right]_{\text{isentropic}} = \left[\frac{\varkappa+1}{2} - \frac{\varkappa-1}{2}\left(\frac{q}{a^*}\right)^2\right]^{\frac{1}{\varkappa-1}} \qquad (1)$$

is changed into an artificial relationship when entering the supersonic region of

$$\left[\frac{\rho}{\rho^*}\right]_{\text{fictitious}} = \left(\frac{q}{a^*}\right)^{-P} \qquad (2)$$

with $q = |\vec{V}|$ representing the velocity vector. Values of $P > 1.0$ result in a hyperbolic type of the equation while values of $P < 1.0$ introduce an elliptic behaviour also in the supersonic region. After [12] values $0.5 \leq P \leq 0.9$ turned out to be reasonable for the calculation process. Doing this a supersonic region without any shockwaves is always achieved. The calculated flowfield outside the airfoil and the supersonic region is elliptical and is governed by the correct equations. The real flowfield inside the supersonic region and the location of the sonic line does not correspond to the airfoil shape due to the application of the fictitious gas law there. As the flowfield in the supersonic region is only influenced by the flow conditions at the sonic line and the location of itself it is now possible to calculate starting from the given sonic line the correct flowfield in the supersonic region by the method of characteristics. The streamline running through the footpoints of the sonic line on the airfoil contour will be the new airfoil shape in this region. Thus the composition of the two flowfields, elliptical flowfield outside, flowfield calculated by the method of characteristics with a new contour inside the supersonic region yields a redesigned airfoil with a completely shockfree pressure distribution. Special smoothing procedures applied to the end of the new contour make sure that a smooth airfoil contour without gaps and steps is achieved.

The method used here for the analysis calculations with the fictitious gas law is based on the FL06 code of Jameson [13]. Experiences with this kind of optimization process showed that values of P = 0.9 [14] provide good starting values for the redesign process. Further details of this procedure can be found in [15].

Thus the optimization process after this method comprehends the following steps:

- Analysis run with the fictitious gas law in the supersonic region for the basic airfoil including viscous effects by adding an appropriate displacement thickness.
- Calculation of the flowfield in the supersonic region by the method of characteristics starting from the sonic line.
- Determination of the new contour in the supersonic region as the streamline running through the starting and end point of the sonic line.
- Construction of the redesigned airfoil by matching the basic airfoil contour with the new one with special smoothing procedures.
- Subtraction of the displacement thickness to get the real airfoil shape.
- Analysis run with the correct gas law to check the design result.

This short description of the principles of the method of elliptic continuation shows that it turns out to be a valuable tool for redesigning airfoils for several new design points with shockfree pressure distributions because the airfoil contour is only changed in a limited region on the upper surface where supersonic flow is present. This property is an important feature for the design of an adaptive airfoil due to two reasons:

- The airfoil contour remains unchanged outside the supersonic region, and

- the actual contour change to achieve shockfree pressure distributions is small ($\Delta y/c < 0.005$).

The type of the shockfree pressure distribution is dependent upon the basic airfoil contour and through the sonic line upon the value P of the fictitious gas law.

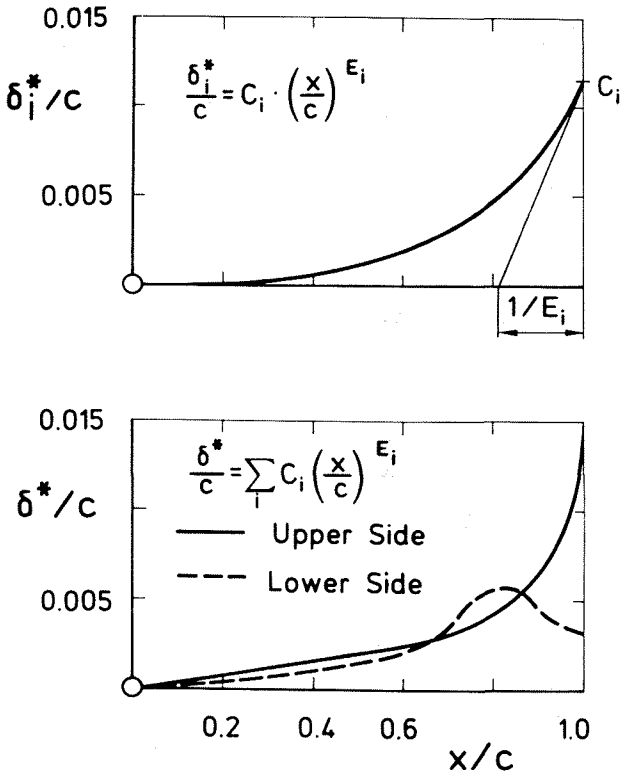

Fig. 3 Scheme of boundary layer displacement thickness model

In order to account for viscous effects also in the redesign process airfoil shapes including the displacement thickness are used during the calculation. The displacement thicknesses along the airfoil contour are modelled by generalized parabolas as schematically shown in Fig. 3. The superposition of a set of parabolas provides reasonable displacement thicknesses for upper and lower surfaces of airfoils as shown in Fig. 3, too. The real contour then can be generated by subtracting the displacement thickness from the viscous contour. As in the redesign process only shockfree pressure distributions are considered, no care of shock boundary layer interaction has to be taken into account.

4. Design process and airfoil analysis

As explained in the previous chapter a basic airfoil is necessary for the application of the method of elliptic continuation. For the purpose of this study the airfoil DFVLR-R44S has been chosen as basic airfoil. It represents a modification of the airfoils DFVLR-R4 [16] and DFVLR-R4/4 [17] which are transonic airfoils of 13.5% thickness and serve as basic sections of a transonic wing. The design point of the airfoil DFVLR-R44S is at M = 0.73 and c_l=0.6.

In order to extend the application range of this airfoil the upper surface contour should be redesigned in such a manner that shockfree pressure distributions in the Mach number range $0.71 \leq M \leq 0.75$ can be achieved. The corresponding lift coefficients should be varied by the expression

$$M^2 \cdot c_l = \text{const.} = 0.3197$$

prescribing a constant lift force when changing the Mach number. For the adaptive airfoil three Mach numbers have been selected which lead to the following design points:

Design Point	M	c_l	Airfoil
①	0.71	0.634	DFVLR-A71
②	0.73	0.600	DFVLR-A73
③	0.75	0.568	DFVLR-A75

The Reynolds number of the numerical study was fixed at $Re = 10 \cdot 10^6$ with transition fixed at 7% on upper and lower surface.

	M	c_l	c_d	Remarks
---	0.71	0.634	0.0091	
——	0.73	0.600	0.0091	Design. Point
—·—	0.75	0.568	0.0100	

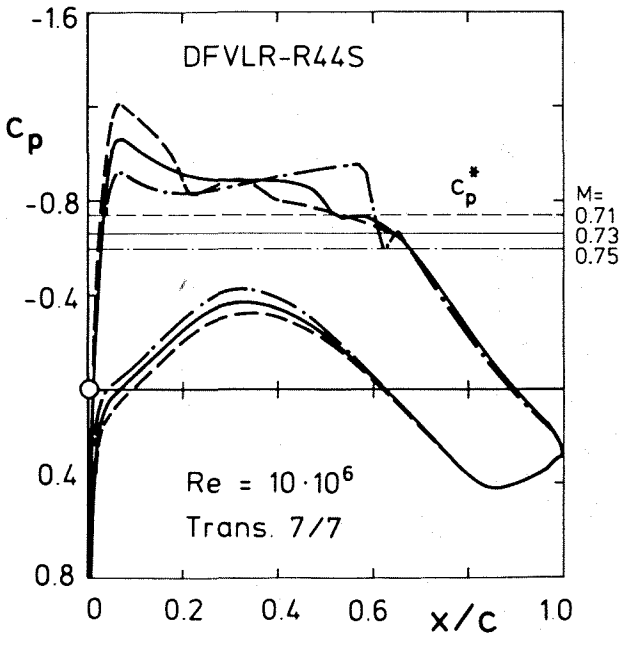

Fig. 4 Pressure distribution of the airfoil DFVLR-R44S at three Mach numbers for the design lift coefficients (BGKJ-method)

Fig. 4 presents calculated pressure distributions after the method of Bauer/Garabedian/Korn/Jameson (BGKJ) [18,19] including viscous corrections after the Nash/Macdonald [20] method for the basic airfoil at the three design points. At M = 0.71 and M = 0.75 shockwaves can be seen whereas at M = 0.73 only a weak disturbance at x/c=0.5 on the upper surface is present. Through the optimization process all three pressure distributions are aimed for becoming shockfree. The optimization process for all three airfoils is exemplarily described for the case of the second airfoil DFVLR-A73 at M = 0.73. As the pressure distribution for this design condition is very near to a shockfree one (Fig. 4) a first optimization cycle was started with the basic airfoil contour. Fig. 5 presents a shockfree pressure distribution obtained in an analysis run by the viscous BGKJ-method. The figure below the pressure distribution gives an indication of the contour modification necessary to achieve this aim. Although a shockfree recompression has been achieved the pressure distribution is not satisfactory due to the concave character indicated by the attached tangent. Experimental experiences show that such a type of pressure distribution in the supersonic region tends to break down forming a shockwave. Therefore a further design step was done making use of the possibilities to influence the pressure distribution as mentioned in the previous chapter by changing the sonic line. This can be achieved by two ways:

- Changing the exponent P in equation (2) for the fictitious gas law or
- changing the contour of the basic airfoil in the expected supersonic region.

For the purpose of this study the second choice was made. The optimization code provides an easy way to add busters or bumps to the basic contour, thus influencing the pressure distribution in the desired way. For an adaptive airfoil this can only be done in the expected region of the supersonic flow on the airfoil.

In a further design step a proper buster was applied to the contour and the design process was repeated. The result is shown in Fig. 6 with the indication of the surface modification. The presented pressure distribution of this design step is also shockfree and looks favourable due to a slight convex type of pressure distribution. This modification was selected as the second design point of the adaptive airfoil, DFVLR-A73.

Equivalent procedures for the two other design points yield the two airfoils DFVLR-A71 and DFVLR-A75 [21]. The analysis runs for the three airfoils at their design points are presented in Fig. 7 and show for all three cases shockfree pressure distributions which develop in a special manner.

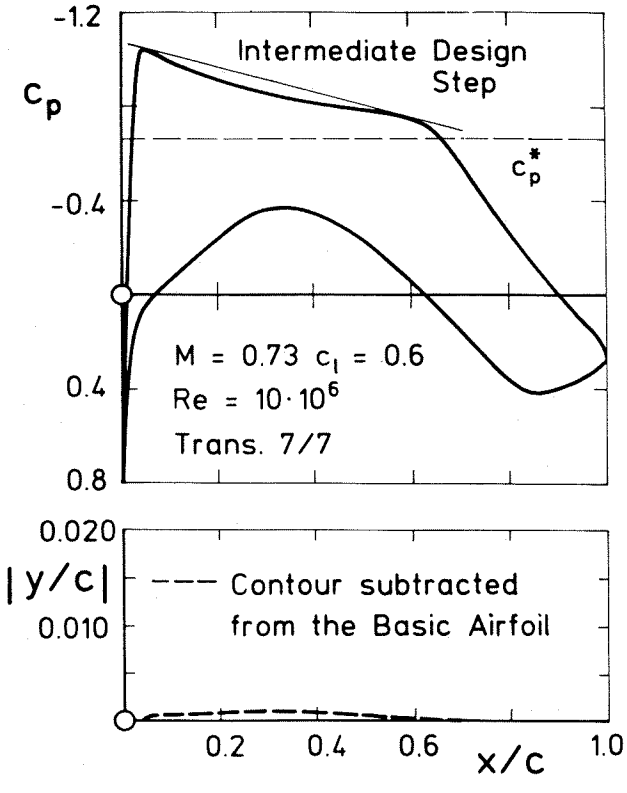

Fig. 5 Calculated pressure distribution by BGKJ-method and contour modification relative to the basic airfoil of the first design run

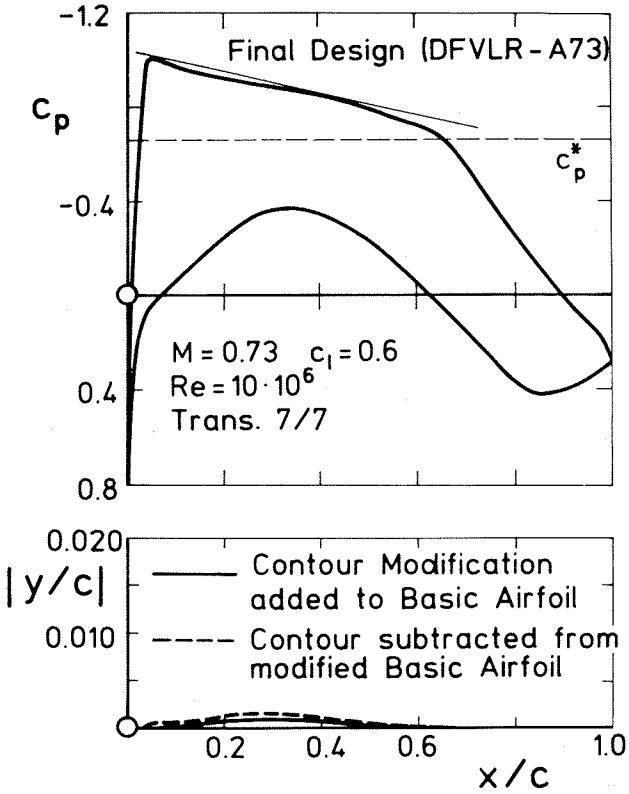

Fig. 6 Calculated pressure distribution by BGKJ-method and contour modification, relative to the basic airfoil of the final design run

At M = 0.71 a more peaky type of pressure distribution is present with a moderate length of supersonic flow which tends to change at M = 0.73 to a more sloping rooftop and at M = 0.75 a long supersonic rooftop pressure distribution is achieved up to x/c = 0.7. According to this variation the surface contour modifications for the three airfoils are presented in Fig. 8. One can see that contour changes only occur in a limited region of the upper surface. The airfoil DFVLR-A73 has only a very small contour change due to the fact that the pressure distribution of the basic airfoil for this case (Fig. 4) is nearly shock-free. The largest modification is presented for the airfoil DFVLR-A75.

	M	c_l	c_d	Airfoil
----	0.71	0.634	0.0089	DFVLR-A71
——	0.73	0.600	0.0091	DFVLR-A73
—·—	0.75	0.568	0.0094	DFVLR-A75

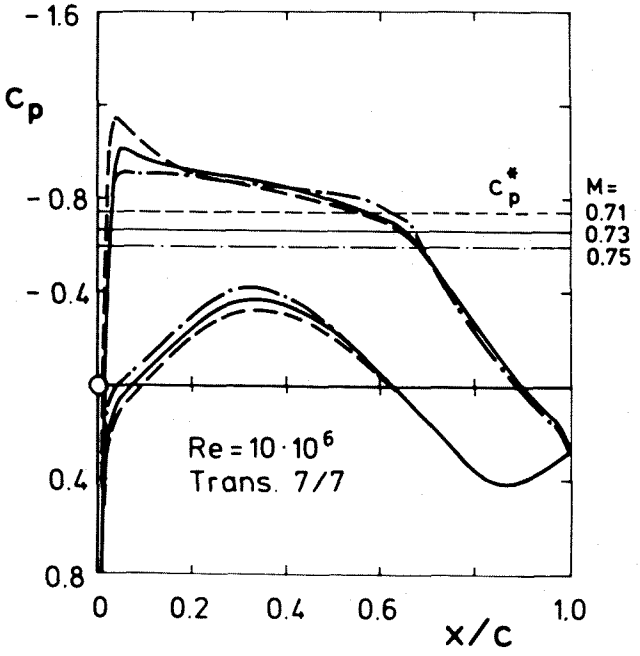

Fig. 7 Pressure distribution of the adaptive airfoil at three Mach numbers for the design conditions (analysis by BGKJ-method)

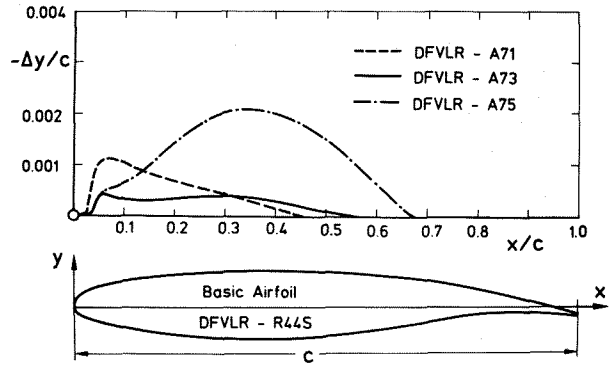

Fig. 8 Contour modifications of the three designed airfoils, relative to the basic airfoil

Extensive analysis runs for all airfoils have been performed with the BGKJ-method and the results for the drag polars of all three airfoils for the Mach numbers M=0.71, 0.73 and 0.75 are presented in Fig. 9. It comes out that the airfoil DFVLR-A71 gives the best results concerning drag for the Mach numbers M = 0.71 and M = 0.73 mainly resulting from a smaller wave drag at high lift coefficients also plotted in Fig. 9. At M = 0.75 the airfoil DFVLR-A75 has the best performance near the design lift coefficient which is also a consequence of a lower wave drag coefficient for this airfoil.

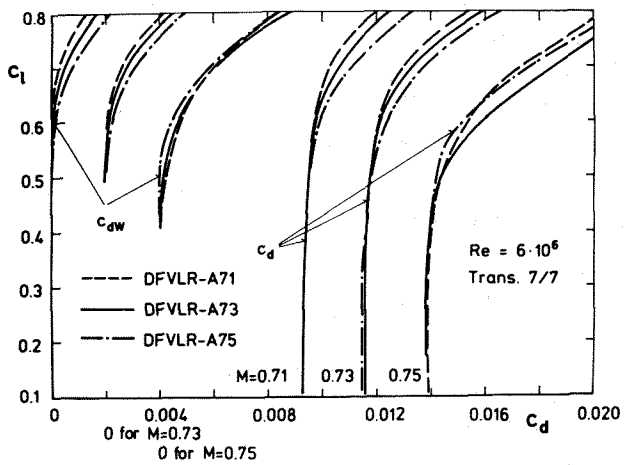

Fig. 9 Calculated drag polars for the adaptive airfoil at the design Mach numbers

Dragrise curves for the three airfoils DFVLR-A71, A73 and A75 and also for the basic airfoil DFVLR-R44S have been derived from the polars and are plotted in Fig. 10. It turns out that the desired extension of the flight envelope did not occur at all M-c_l-combinations as expected in its full entirety presented in Fig. 1. Fig. 10 shows that for the airfoil DFVLR-A73 no improvement in dragrise compared to the basic airfoil DFVLR-R44S has been achieved. In the Mach number region M < 0.75 the expected extension of the flight regime is predicted by the better performance of the airfoil DFVLR-A71, which is also nearly the same at M ≈ 0.75 as for the airfoil DFVLR-A73. In the low lift coefficient region the expected shift of the dragrise curve to higher Mach numbers for the airfoil DFVLR-A75 did not occur, only a small benefit can be seen near the design lift coefficient of $c_l \approx 0.55$. The reason for this behaviour at low c_l might be due to the long extension of the supersonic region on this airfoil leading to shockwaves at low lift coefficients which influence the dragrise unfavourable.

In order to clarify this situation an experimental program was initiated.

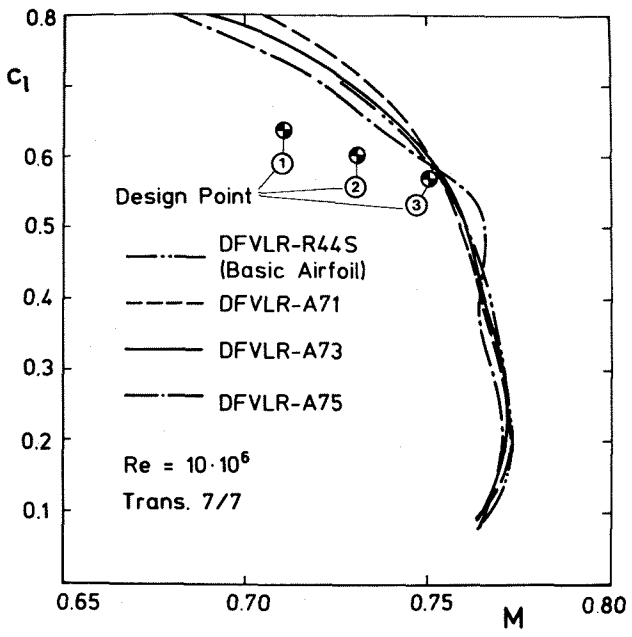

Fig. 10 Calculated dragrise curves ($\Delta c_{d,M=0.6}=0.002$) for the basic airfoil and for the adaptive airfoil

5. Experimental Results

The experimental results were obtained in the Transonic Windtunnel of DFVLR Braunschweig (TWB) [22], which is a blowdown windtunnel (Fig. 11) and especially suited for airfoil investigations at transonic speeds ($0.4 \leq M \leq 0.95$). The rectangular test section (34 cm x 60 cm) with slotted top and bottom walls (2.35% open area ratio) allows to test airfoil models of 15 cm chord length up to Reynolds numbers of $Re = 1.4 \cdot 10^7$. Lift and pitching moment coefficients are evaluated from static pressure measurements on the airfoil surface whereas drag coefficients are calculated from wake traverse measurements.

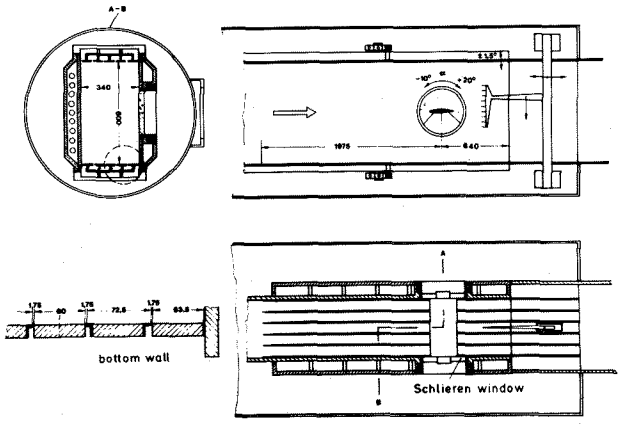

Fig. 11 Transonic Windtunnel Braunschweig (TWB) of DFVLR

Three models of 15 cm chord length of the designed airfoils DFVLR-A71, A73, A75 have been manufactured with an accuracy in contour of approximately 0.02 to 0.03 mm. Such high accuracy is required for this set of models because the smallest contour differences between the airfoils are according to Fig. 8 in the order of 0.06 mm.

The model tests have been performed at a Reynolds number of $Re = 6 \cdot 10^6$ which is a reasonable compromise between economic windtunnel operation and the demand for sufficient high Reynolds numbers. This Reynolds number is normally used for airfoil tests in the TWB. The tests were all carried out with free transition although the design calculations have been performed with transition fixed at 7% on the upper and lower surface. It seems not to be worthwhile to do the tests with transition fixed due to the following reasons:

- Transition strips normally generate additional drag. As it is nearly impossible to reproduce a transition strip, the comparison of drag coefficients of different airfoils is often questionable.
- The transition strip is disturbing the pressure distribution at the beginning of the supersonic region on the upper surface and thus influencing the development of the pressure on the whole airfoil.

A comprehensive test program for all three airfoils has been carried out at Mach numbers of $0.6 \leq M \leq 0.79$ and lift coefficients of $0.1 \leq c_l \leq c_{l_{max}}$ in order to determine the performance boundaries. Only selected results, comprehending pressure distributions, drag polars and performance boundaries will be presented. Detailed discussions on the experimental results are beyond the scope of this paper.

Pressure distributions at the design Mach numbers and nearby the design lift coefficients are plotted together with the corresponding calculated results in Fig. 12 to 14. Fig. 12 shows the pressure distributions of the airfoils DFVLR-A71, A73 and A75 at $M = 0.71$ and $\alpha = 1.5°$ as obtained in the windtunnel in comparison with those calculated for nearly the same lift coefficients. These lift coefficients c_l are very near to the design value for the airfoil DFVLR-A71 at this Mach number of $c_{l_D} \approx 0.634$. Looking at the experiments one can state that at the lower surface nearly the same pressure distribution has been measured for all three airfoils. On the upper surface characteristic differences occur in the development of the supersonic region and in the pressure curves up to $x/c \approx 0.7$. In all three cases shockwaves appear and no shockfree solution has been measured for the design case of the DFVLR-A71 airfoil. But this airfoil has the smallest supersonic region and the weakest shockwave which leads to the lowest drag coefficient. For the airfoil DFVLR-A75 the largest supersonic region with the strongest shockwave

	c_l	c_d	Airfoil
----	0.616	0.0099	DFVLR-A71
———	0.633	0.0103	DFVLR-A73
—·—	0.643	0.0102	DFVLR-A75

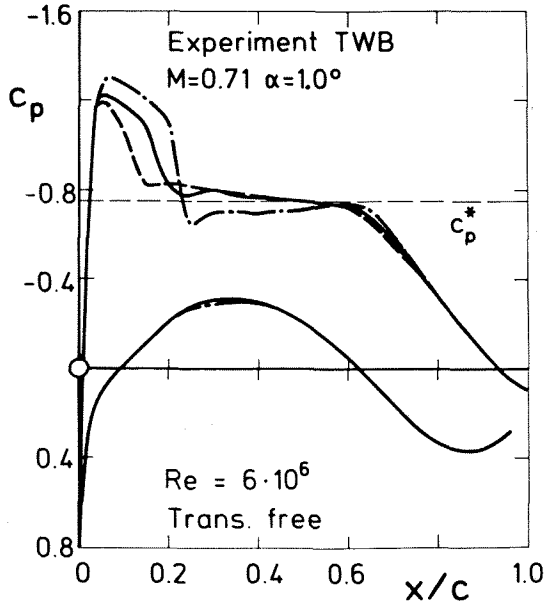

	c_l	c_d	Airfoil
----	0.633	0.0098	DFVLR-A71
———	0.634	0.0099	DFVLR-A73
—·—	0.626	0.0101	DFVLR-A75

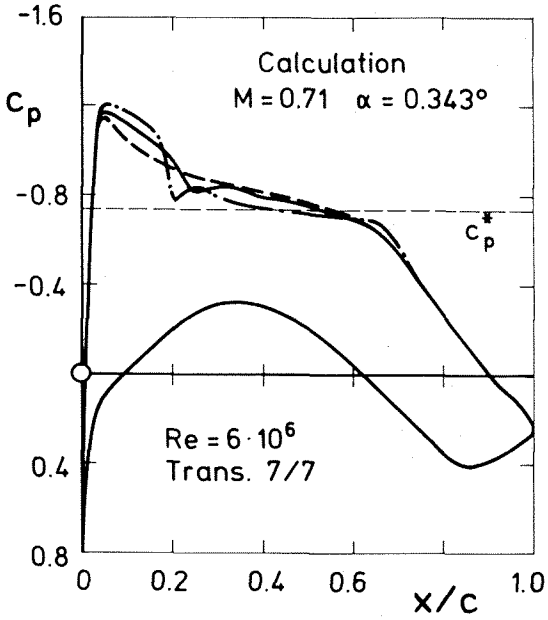

Fig. 12 Measured and calculated pressure distributions of the adaptive airfoil at the design Mach number M = 0.71

	c_l	c_d	Airfoil
----	0.559	0.0103	DFVLR-A71
———	0.573	0.0101	DFVLR-A73
—·—	0.571	0.0106	DFVLR-A75

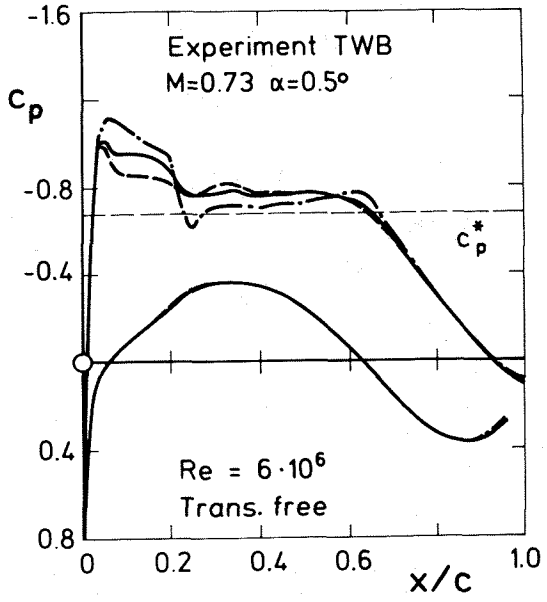

	c_l	c_d	Airfoil
----	0.569	0.0099	DFVLR-A71
———	0.569	0.0100	DFVLR-A73
—·—	0.560	0.0100	DFVLR-A75

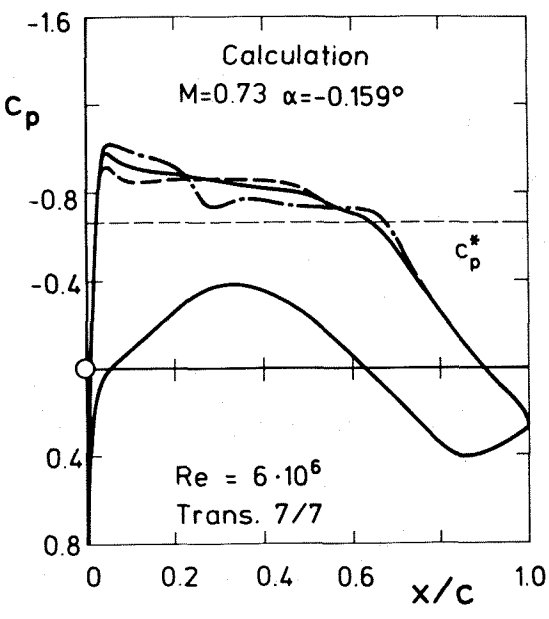

Fig. 13 Measured and calculated pressure distributions of the adaptive airfoil at the design Mach number M = 0.73

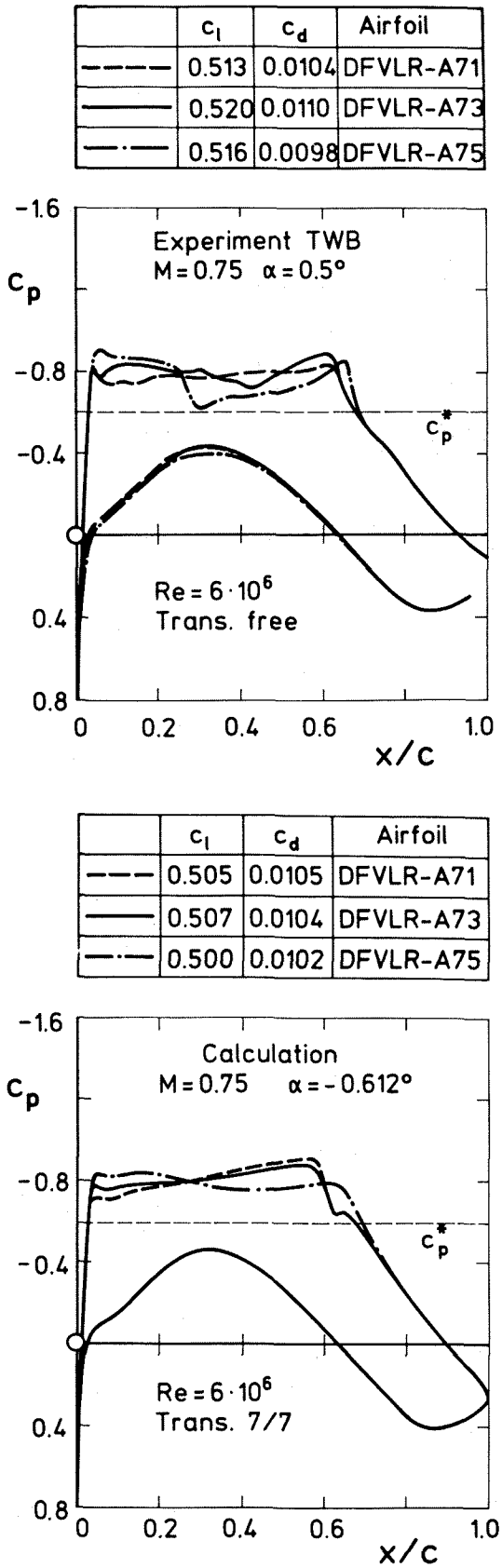

Fig. 14 Measured and calculated pressure distribution for the adaptive airfoil at the design Mach number M = 0.75

has been measured connected with the highest drag coefficient. Comparing the measured pressure distributions of the three airfoils with the calculated ones it can be seen that apart from the fact that no shockfree solution has been obtained in the tests the calculations are in good agreement with experiments with regard to typical differences in pressure distributions such as leading edge suction peak, development and beginning of the strong recompression at $x/c \approx 0.65$.

The same situation at M = 0.73 and $\alpha = 0.5°$ is given in Fig. 13. The pressure distributions of the airfoils DFVLR-A71 and A73 show a nearly shockfree behaviour with only minor disturbances at lift coefficients of $c_l \approx 0.57$ which is a little bit lower than the design value of $c_{lD} = 0.6$ for M = 0.73. The pressure distribution of the airfoil DFVLR-A75 shows a shockwave at x/c = 0.2 on the upper surface, a re-expansion and a longer supersonic region with a more pronounced recompression in the region of $x/c \approx 0.65$. The measured drag values differ only by a small amount of $\Delta c_d \approx 0.0004$. This typical behaviour of the measured pressure distribution has been also predicted by theoretical calculations with regard to the suction peak development, shockwave occurrence and differences in length of the supersonic regions.

For the Mach number M = 0.75 and $\alpha = 0.5°$ measured and calculated pressure distributions for lift coefficients of $c_l \approx 0.5$ which is lower than $c_{lD} = 0.569$ are presented in Fig. 14. For the airfoils DFVLR-

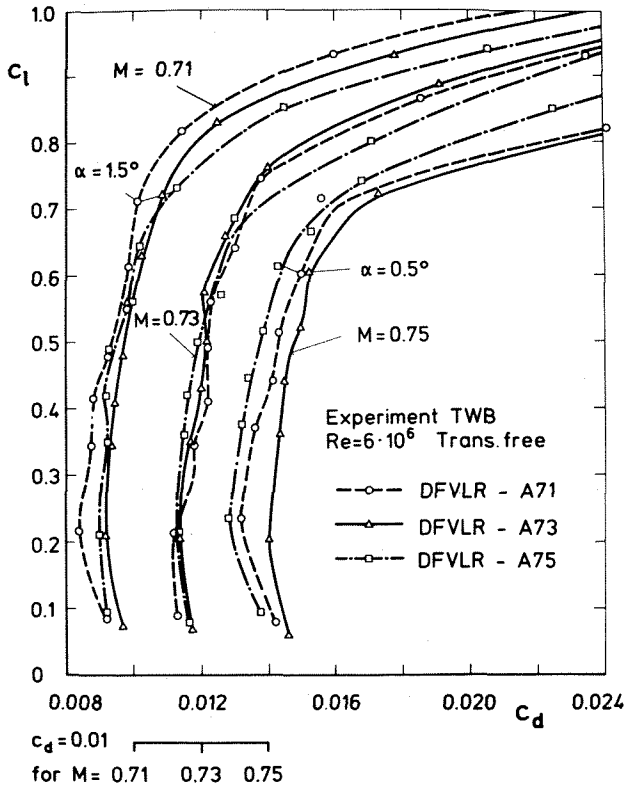

Fig. 15 Comparison of measured drag polars

A71 and A73 supersonic rooftop pressure distributions with a slight expansion ended with a shockwave have been measured. The optimized airfoil for this Mach number DFVLR-A75 develops a double shocksystem with a long supersonic region. With regard to the drag coefficients the latter type of pressure distribution gives the smallest one. This can only be explained by a favourable influence of transition location and the boundary layer development. The general agreement between measured and calculated pressures is not as good as for the other two Mach numbers of M = 0.71 and 0.73.

The drag polars of the three airfoils at the Mach numbers M = 0.71, 0.73 and 0.75 are plotted together in Fig. 15. This figure can be compared with calculated results from Fig. 9. The polars for the Mach numbers M = 0.71 and M = 0.73 show nearly the same behaviour as predicted by the calculations, although the absolute values differ. In the lower lift coefficient region the drag coefficients of the three airfoils differ only about approximately $\Delta c_d \approx 0.0005$ whereas the calculations show a constant drag value. These differences in measured drag values may have the following reasons:

- The accuracy of measured drag coefficients from the wake traverse is in the order of $\Delta c_d = \pm 0.0002$,
- the measurements have been performed with free transition. Thus differences in transition location result in a drag difference.

At higher lift coefficients $c_l \geq 0.65$ it turns out that for M = 0.71 the airfoil DFVLR-A71 has the lowest drag values where-

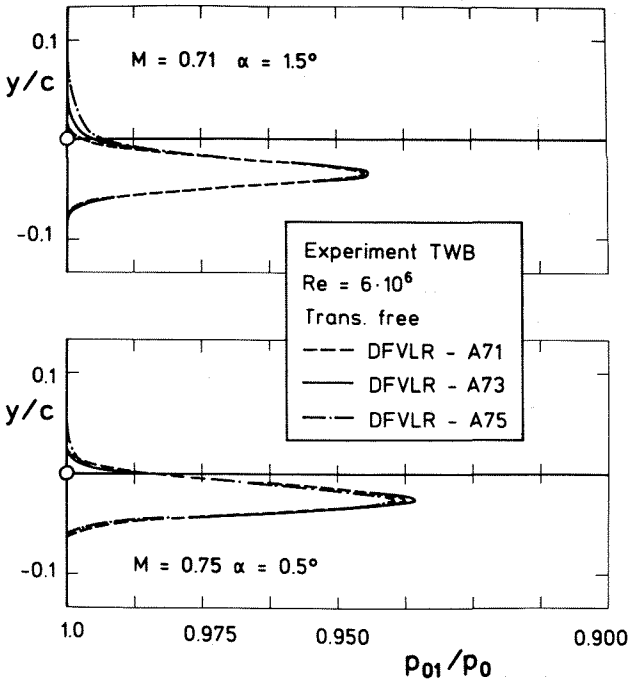

Fig. 16 Comparison of total pressure loss in the wake one chord length behind the airfoil

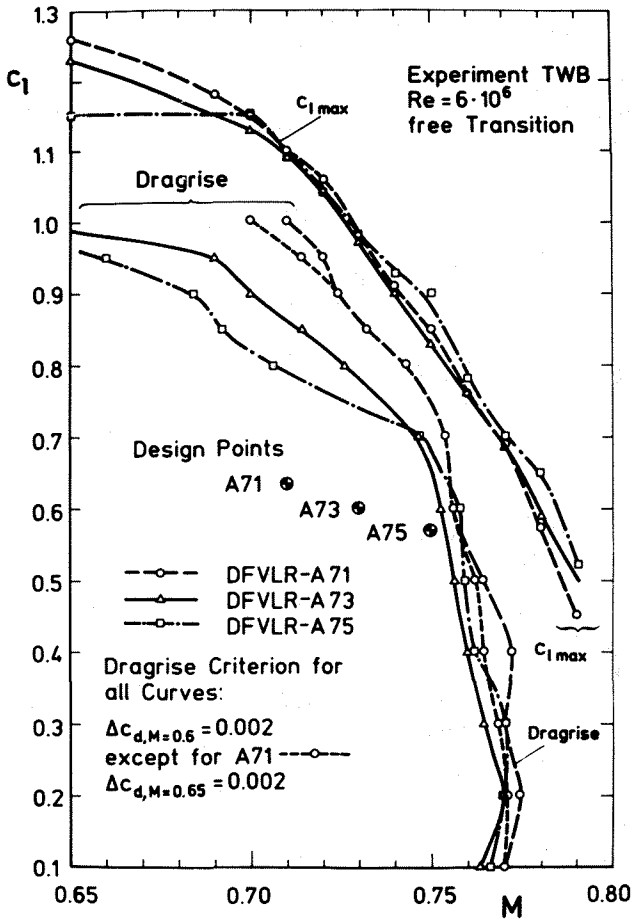

Fig. 17 Maximum lift and dragrise boundaries of the adaptive airfoil in its three design conditions

as at M = 0.73 the airfoils DFVLR-A71 and A73 have equal drag coefficients. For both Mach numbers the airfoil DFVLR-A75 provides the highest c_d-value. This is in accordance with the predicted behaviour. At M = 0.75 significant drag differences already appear at low lift coefficients in contrast to the calculations. It is assumed that remarkable differences in transition location on upper and lower surface are responible for this behaviour which might be due to surface contamination. The airfoil DFVLR-A75 shows the lowest drag values for the whole polar. This is also in contrast to the calculations.

In order to gain a deeper insight the total wake pressures for two cases which are marked in Fig. 15 (M = 0.71, $\alpha = 1.5°$ and M = 0.75 and $\alpha = 0.5°$) are compared in Fig. 16. For the first case (M = 0.71 and $\alpha = 1.5°$) the drag differences can be appointed to differences in the wake total pressure on the upper surface resulting from different shock strengths. In accordance with the calculations in Fig. 9 the airfoil DFVLR-A71 has the lowest wave drag and the airfoil DFVLR-A75 the highest one. The second case (M = 0.75 and $\alpha = 0.5°$) shows a different behaviour. The total pressures in the wake of the three airfoils mainly differ in the region of the minimum

value. This behaviour can be attributed to a different development in boundary layer coming from a variation in transition location on the upper and lower surface. These effects have not yet fully understood and further investigations concerning transition have to be carried out.

Measured performance boundaries of the three airfoils as dragrise and maximum lift coefficients versus Mach number have been plotted in Fig. 17. At Mach numbers $M < 0.7$ the airfoil DFVLR-A71 has the highest $c_{l_{max}}$-values, whereas the airfoil DFVLR-A75 shows the lowest ones. In the region of $0.7 \leq M \leq 0.79$ $c_{l_{max}}$-values of the airfoils DFVLR-A71 and A73 are nearly the same. The airfoil DFVLR-A75 indicates two regions of higher $c_{l_{max}}$-values: around $M \approx 0.75$ and $M \approx 0.77$. The dragrise curves of the three airfoils show nearly the same tendencies as predicted in the calculations (Fig. 10). An extension of the flight regime due to the airfoil DFVLR-A71 to higher lift coefficients at Mach number $M \leq 0.75$ can be stated. At greater Mach numbers $M \geq 0.75$ the dragrise curves only differ in Mach number of $\Delta M \approx 0.01$, whereby the airfoil DFVLR-A73 always tends to the lower Mach number. The predicted extension of flight regime for the airfoil DFVLR-A75 at lift coefficients $c_l \approx 0.5$ to 0.55 can hardly be seen at $c_l \approx 0.6$. As the dragrise curves are derived with the increment criterion small differences in drag values at $M = 0.6$ may influence the dragrise Mach numbers. This can be seen for the airfoil DFVLR-A71 which has an extremely high dragrise Mach number at c_l-values of $c_l \approx 0.4$. If the Mach number $M = 0.65$ is chosen as reference for the drag increment a reasonable approximation to the curves of the other two airfoils takes place. From this figure one clearly can state that only a remarkable extension in flight regime to higher lift coefficients has been achieved. A shift of the dragrise curve to higher Mach numbers in the low lift coefficient region with the aid of the airfoil DFVLR-A75 has not been achieved apart from a very small region near $c_l = 0.6$. This is mainly due to the fact that all three dragrise curves include all three design points into the flight regime, inspite of the prediction made in Fig. 1.

The dragrise curves and the $c_{l_{max}}$-boundaries are not the only factors determining airfoil performance. Another important parameter is the airfoil efficiency $M \cdot c_l/c_d$ which is plotted for the three airfoils in a lift coefficient Mach number diagram in terms of lines with constant $M \cdot c_l/c_d$ in the Fig. 18 to 20. Highest values of this airfoil efficiency indicate regions of best airfoil performance. Apart from differences in the curves which are present for the three airfoils one common feature can be stated. The best performances of the airfoils are not achieved in the estimated shockfree design conditions which are marked in the figures, but appear at higher lift coefficients, where shockwaves are present. This can be explained by the fact that the

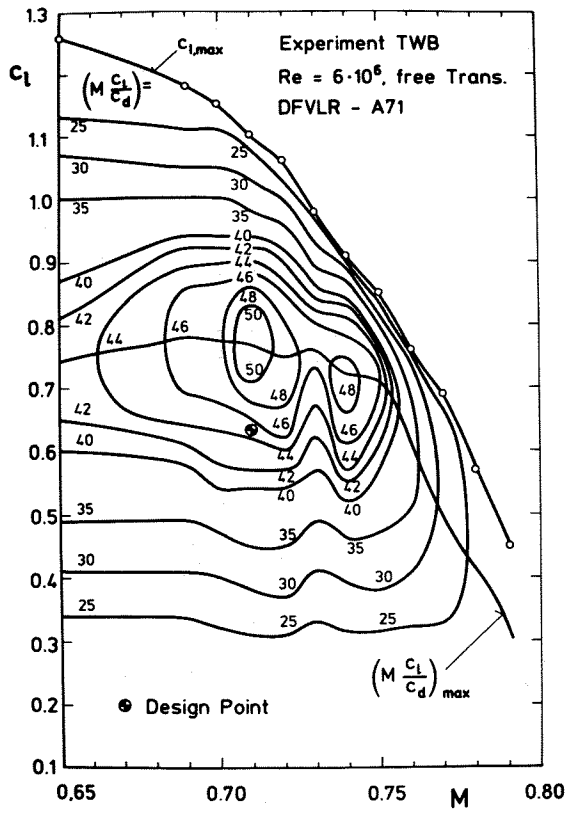

Fig. 18 Measured aerodynamic efficiency of the adaptive airfoil DFVLR-A71

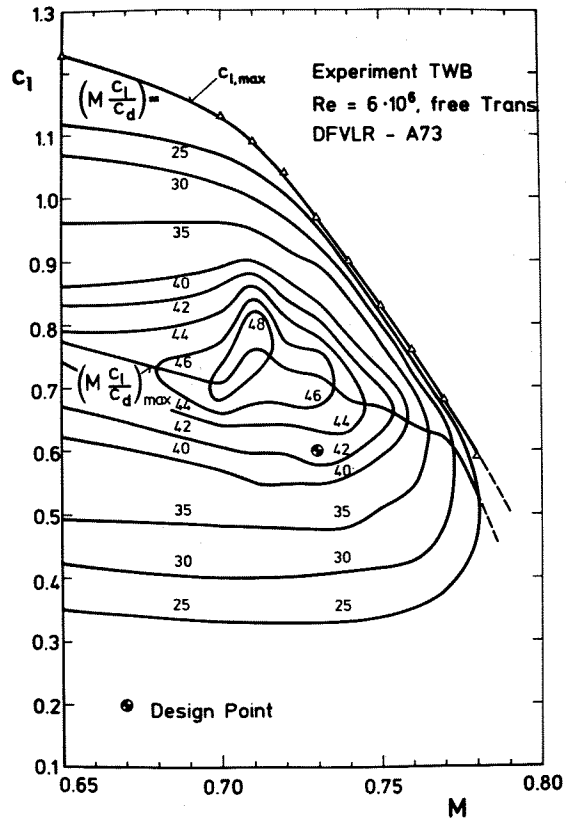

Fig. 19 Measured aerodynamic efficiency of the adaptive airfoil DFVLR-A73

gain in lift with the occurrence of shockwaves is greater than the increase of drag coefficients due to shockwaves.

Looking at Fig. 18 (airfoil DFVLR-A71) two regions of highest airfoil efficiency can be found: one at M = 0.71 and $c_l \approx 0.75$ ($M \cdot c_l/c_d = 50$), the other at M = 0.74 and $c_l \approx 0.7$ ($M \cdot c_l/c_d = 48$). At M = 0.73 a certain breakdown in airfoil efficiency occurs which is not fully understood now. The airfoil efficiency of the DFVLR-A73 (Fig. 19) is only higher compared to Fig.18 (DFVLR-A71) at M = 0.73 and c_l-values around $c_l \approx 0.7$ although the maximum value also is reached at M = 0.71. Fig. 20 explains the situation for the third airfoil (DFVLR-A75). Compared to the airfoil DFVLR-A71 an improvement in airfoil efficiency can only be found at M = 0.75 and lift coefficients around $c_l \approx 0.67$ ($M \cdot c_l/c_d = 46$). This is the maximum value for this airfoil.

6. Conclusions

Summarizing the results of these investigations the following statements can be made:

- The elliptic continuation method is a valuable tool for designing airfoils with shockfree pressure distributions.
- For a basic airfoil different upper surface contours corresponding to different flow conditions can be designed with shockfree pressure distributions representing an adaptive airfoil.
- Shockfree pressure distributions for these conditions could be confirmed in analysis runs.
- Calculated dragrise curves revealed that an extension of the flight regime by an adaptive airfoil could not be confirmed in the anticipated range of Mach numbers and lift coefficients.
- Experimental results indicate that shockfree pressure distributions could hardly be obtained.
- The maximum airfoil efficiency was not obtained at flow conditions having no shockwaves or small weak shocks but with pressure distributions with weak to moderate shockwaves at higher lift coefficients than the prescribed design values.
- An extension of the flight regime with high aerodynamic efficiency with the aid of the adaptive airfoil could be confirmed for the range of Mach numbers M < 0.75 where the experimental dragrise curve was shifted to higher lift coefficients.
- No great effect could be experimentally verified in shifting the dragrise curve to higher Mach numbers at low lift coefficients for the special higher Mach number design point.
- One of the investigated airfoils (DFVLR-A71) turns out to have nearly the best performance at all flight conditions except some singular points compared with the performances of the other two airfoils.
- Thus these investigations revealed that an adaptive airfoil seems not to be conclusive for the case considered here, because most of the advantages could be achieved by an airfoil designed for one point. This might be due to the fact that the prescribed design points for all designed airfoils lie well within the economic flight regime below the dragrise curves. The situation may be different for airfoil types which are extreme in their design conditions (e.g. at dragrise or very near to it) but for this case difficulties in off-design conditions are expected.

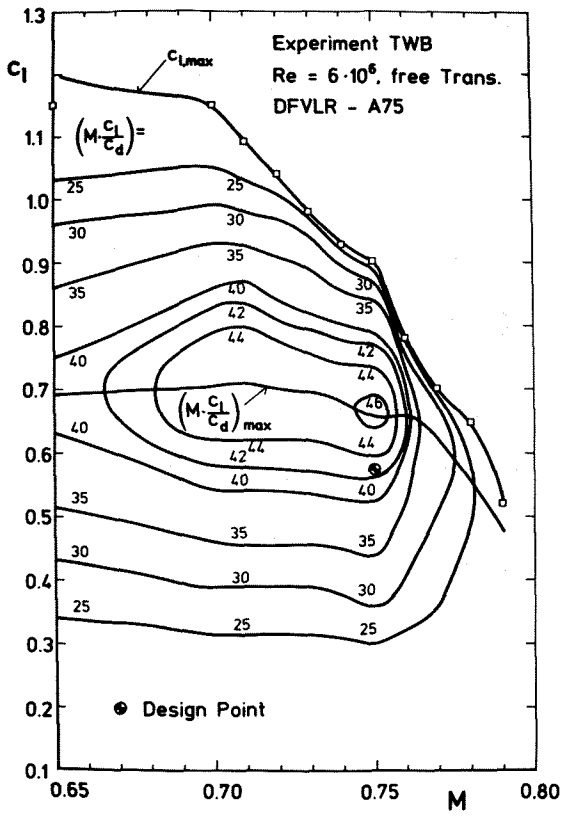

Fig. 20 Measured aerodynamic efficiency of the adaptive airfoil DFVLR-A75

References

[1] Krenz, G., Hilbig, R.: Aerodynamic concepts for fuel-efficient transport aircraft. ICAS-82-1.5.2, Proceedings (1982).

[2] CTOL Transport technology - 1978. NASA CP 2036, Part I, II (1978).

[3] Pope, G.G.: Prospects for reducing the fuel consumption of civil aircraft. Aeron. Journ. 83 (1979), pp. 287-295.

[4] Poisson-Quinton, Ph.: Energy conservation aircraft design and operational procedures. AGARD-LS-96 (1978), pp.9-1 to 9-47.

[5] Krenz, G., Ewald, B.: Transonic wing technology for transport aircraft. AGARD-CP-285 (1980), pp. 12-1 to 12-12.

[6] Redeker, G., Schmidt, N., Müller, R.: Design and experimental verification of a transonic wing for a transport aircraft. AGARD-CP-285 (1980), pp. 13-1 to 13-14.

[7] Körner, H., Redeker, G.: Recent airfoil developments at DFVLR. ICAS-82-5.6.2 Proceedings (1982).

[8] Redeker, G., Müller, R.: Design and experimental verification of two supercritical airfoils. DGLR-Symp. "Transonic Configurations", Bad Harzburg, FRG (1978), DGLR-No. 78-075.

[9] Sobieczky, H., Fung, K.Y., Seebass, A.R.: A new method for designing shockfree transonic configurations. AIAA Paper No. 78-1114 (1978).

[10] Sobieczky, H.: Transonic shockfree design in 3D. DGLR-Symp. "Transonic Configurations", Bad Harzburg, FRG (1978), DGLR-No. 78-066.

[11] Eberle, A.: Transonic potential flow computations by finite elements: airfoil and wing analysis, airfoil optimization. DGLR-Symp. "Transonic Configurations", Bad Harzburg, FRG (1978), DGLR-No. 78-065.

[12] Sobieczky, H.: Design of advanced technology transonic airfoils and wings. AGARD-CP-285 (1980), pp. 10-1 to 10-13.

[13] Jameson, A.: Transonic flow calculations. VKI-LS-87 (1976).

[14] Wichmann, G.: Entwurf eines Basisprofils für einen schwach gepfeilten Tragflügel. DFVLR-IB 129-81/23 (1981).

[15] Sobieczky, H.: Rheograph transformation and continuation methods. VKI-LS-1980-4 (1980).

[16] Redeker, G., Müller, R.: Messungen am Profil DFVLR-R4 im Transsonischen Windkanal Braunschweig. DFVLR-IB 151-78/3 (1978).

[17] Redeker, G., Brandes, H.: Modifikation des transsonischen Profils DFVLR-R4. DFVLR-IB 129-81/24 (1980).

[18] Bauer, F., Garabedian, P., Korn, D., Jameson, A.: Supercritical wing sections II. Lecture Notes in Economics and Math. Syst., Vol. 108 (1975). Springer-Verlag Berlin/Heidelberg/New York.

[19] Bauer, F., Garabedian, P., Korn, D.: Supercritical wing sections III. Lecture Notes in Economics and Math. Syst., Vol. 150 (1977). Springer-Verlag Berlin/Heidelberg/New York.

[20] Nash, J.F., Macdonald, A.G.J.: The calculation of momentum thickness in a turbulent boundary layer at Mach numbers up to unity. ARC C.P. No.963 (1967).

[21] Oelker, H.-Chr.: Entwurf und Nachrechnung eines transsonischen, adaptiven Profils. DFVLR-IB 129-83/8 (1983).

[22] Stanewsky, E., Puffert-Meißner, W., Müller, R., Hoheisel, H.: Der Transsonische Windkanal Braunschweig der DFVLR. Z. Flugwiss. Weltraumforsch. 6 (1982), S. 398-408.